Observed Impact of Atlantic SST Anomalies on the North Atlantic Oscillation

ARNAUD CZAJA

Department of Earth, Atmospheric, and Planetary Sciences, Massachusetts Institute of Technology, Cambridge, Massachusetts

CLAUDE FRANKIGNOUL

Laboratoire d'Oceanographie Dynamique et de Climatologie, Universite Pierre et Marie Curie, Paris, France

(Manuscript received 12 March 2001, in final form 3 August 2001)

ABSTRACT

The large-scale patterns of covariability between monthly sea surface temperature (SST) and 500-mb height anomalies (Z_{500}) in the Atlantic sector are investigated as a function of time lag in the NCEP–NCAR reanalysis (1958–97). In agreement with previous studies, the dominant signal is the atmospheric forcing of SST anomalies, but statistically significant covariances are also found when SST leads Z_{500} by several months. In winter, a Pan-Atlantic SST pattern precedes the North Atlantic oscillation (NAO) by up to 6 months. Such long lead time covariance is interpreted in the framework of the stochastic climate model, reflecting the forcing of the NAO by persistent Atlantic SST anomalies.

A separate analysis of midlatitudes (20°–70°N) and tropical (20°S–20°N) SST anomalies reveals that the bulk of the NAO signal comes from the midlatitudes. A dipolar anomaly, with warm SST southeast of Newfoundland and cold SST to the northeast and southeast, precedes a positive phase of the NAO, and it should provide a prediction of up to 15% of its monthly variance several months in advance. Since the ''forcing'' SST pattern projects significantly onto the tripole pattern generated by the NAO, these results indicate a positive feedback between the SST tripole and the NAO, with a strength of up to $\simeq$25 m K^{-1} at 500 mb or 2–3 mb K^{-1} at sea level. Additionally, a warming of the tropical Atlantic (20°S–20°N), roughly symmetric about the equator, induces a negative NAO phase in early winter. This tropical forcing of the NAO is nearly uncorrelated with and weaker than that resulting from the midlatitudes, and is associated with shorter lead times and reduced predictive skill.

1. Introduction

Climate variability over the North Atlantic sector is dominated, on monthly and interannual timescales, by a modulation in the strength and position of the atmospheric jet stream, known as the North Atlantic oscillation (NAO). The NAO, which is prevalent during winter, governs large changes in surface temperature and precipitation over the Northern Hemisphere (Hurrell 1995), and strongly affects the ocean through latent and sensible heat exchanges (Cayan 1992). As the resulting sea surface temperature (SST) anomalies have in turn a persistent influence on the air–sea heat fluxes (Frankignoul et al. 1998), there is a substantial thermal coupling between the wintertime oceanic mixed layer and the atmosphere. This may result in a predictable oceanic influence on the NAO.

This influence is however difficult to estimate in observational studies, because the dominant interaction between the atmosphere and the ocean in the extratropics is the forcing of the latter by the former. Frankignoul and Hasselmann (1977) have pointed out that unlagged correlation between SST and atmospheric anomalies were primarily reflecting the atmospheric forcing of the ocean, so that the oceanic influence on the atmosphere can only be established by studying their covariability when the ocean is leading. In most previous studies (e.g., Namias 1964; Ratcliffe and Murray 1970; Deser and Timlin 1997), the focus was on 1-month lead and no significant oceanic impact could be detected. We believe that this reflects in part that large-scale patterns like the NAO have a significant intrinsic persistence, so that the covariability at 1-month lead is still affected by the atmosphere forcing the ocean. In a recent study, Czaja and Frankignoul (1999, hereafter CF99) systematically considered lead times longer than a month, and stratified the analysis by sets of three successive months. Using a maximum covariance analysis (MCA), they found a predictive skill of atmospheric anomalies in two seasons. In late spring, a circulation anomaly over the Hudson Bay was found to be related to SST anomalies in the previous winter, and in early winter the NAO was found to be related to SST anomalies in the previous summer.

Corresponding author address: Dr. Arnaud Czaja, Department of Earth, Ocean and Planetary Sciences, Massachusetts Institute of Technology, Rm 54-1421, 77 Massachusetts Avenue, Cambridge, MA 02139.
E-mail: czaja@ocean.mit.edu

Modeling studies with atmospheric general circulation models (AGCMs) suggest that SST anomalies in the Atlantic sector might indeed have a significant impact on the NAO during winter. Rodwell et al. (1999), Mehta et al. (2000), Latif et al. (2000), Robertson et al. (2000), and Hoerling et al. (2000) were able to reproduce some of the low-frequency variability of the NAO during the last decades from the time history of observed SST anomalies. Rodwell et al. argued that a positive feedback between a tripolar North Atlantic SST pattern and the NAO was responsible for this oceanic influence. Similar conclusion was reached by Watanabe and Kimoto (2000). However, Latif et al. (2000) and Hoerling et al. (2001) suggested that the bulk of the oceanic influence on the NAO might come from the tropical belt, excluding the Atlantic sector. Robertson et al. (2000) argued that tropical and subtropical South Atlantic SST anomalies could play a role as well. These controversial results emphasize that the response of AGCMs to prescribed SST anomalies is strongly model-dependent (see Robinson 2000 for a recent review), stressing the need for further observational studies.

As pointed out by Bretherton and Battisti (2000), the realistic simulation of the low-pass NAO index in the above AGCM studies does not imply predictability of the NAO on decadal timescales (but see also Czaja and Marshall 2000), even if SST anomalies impact the atmospheric flow on short (monthly) timescales. It is precisely this short timescale interaction that we investigate in this paper, using the National Centers for Environmental Prediction–National Center for Atmospheric Research (NCEP–NCAR) reanalysis. By separately applying the MCA to midlatitude and tropical SST anomalies, it will be shown that the bulk of the SST influence on the NAO revealed in CF99 results from local atmosphere–ocean interactions over the North Atlantic, but that there is also a weaker impact on the NAO from tropical Atlantic SST anomalies. The paper is structured as follows. We describe the data and method used in section 2, and a general description of the MCA results is given in section 3. The SST forcing of the NAO is investigated in sections 4 and 5, where a separate MCA is applied to midlatitude and tropical SST anomalies. The implication of our results for NAO predictability on monthly timescales is discussed in section 6. Conclusions are offered in section 7.

2. Data and method

The data used for this study come from the NCEP–NCAR reanalysis (Kalnay et al. 1996). Several atmospheric variables were considered with comparable results, including sea leval pressure, surface wind stress, and low-level temperature, so for brevity we focus on the geopotential height at 500 mb (hereafter Z_{500}). The domain retained for Z_{500} is 20°S–70°N, 100°W–20°E on a 2.5° × 2.5° grid, while the SST data cover the Atlantic basin from 20°S to 70°N on a 1.875° × 1.875° grid. Monthly anomalies over the period 1958–97 (40 yr) were constructed by substracting the mean seasonal cycle from the monthly data. At each grid point, a third-order polynomial was then removed by least squares fit from the anomaly time series, removing the trends and low frequencies displayed in the analysis period.

To investigate how the atmospheric circulation is related to SST anomalies in lead and lag conditions, we are mainly using the MCA. This technique is based on a singular value decomposition (SVD) of the temporal covariance matrix between SST and an atmospheric variable at a given lag, and as such has sometimes been called ''SVD'' analysis in the literature (e.g., Bretherton et al. 1992). To construct the covariance matrix, the monthly anomalies are weighted by the square root of the cosine of latitude, which ensures that equal areas are given equal weight in the analysis. To give similar weight to each month, hence increase the effective number of degrees of freedom, monthly anomalies are normalized by a mean (domain averaged) seasonal cycle of standard deviation. No time filtering or spatial smoothing is applied. The covariance matrix is estimated with monthly anomalies binned into groups of 3 months (i.e., the length N of the time series is usually $N = 3 \times 39$ yr).

In the MCA, say Z_{500} at time t and SST at time $t + \tau$ are expanded into K orthogonal signals:

$$Z_{500}(x, t) = \sum_{k=1}^{K} \mathbf{u}_k(x)\mathbf{a}_k(t) \tag{1}$$

$$\mathrm{SST}(x, t + \tau) = \sum_{k=1}^{K} \mathbf{v}_k(x)\mathbf{b}_k(t + \tau) \tag{2}$$

plus noise, where the covariance between $\mathbf{a}_k(t)$ and $\mathbf{b}_k(t + \tau)$ is the kth singular value of the covariance matrix between SST and Z_{500}, decreasing for increasing k. So-called (Bretherton et al. 1992) homogeneous maps for the ocean and heterogeneous maps for the atmosphere [i.e., the projection of SST $(x, t + \tau)$ and $Z_{500}(x, t)$ onto $\mathbf{b}_k(t + \tau)$] will be shown since they preserve linear relations between the variables (see appendix A). The maps are scaled to represent the amplitude of SST and Z_{500} anomalies associated with one standard deviation of $\mathbf{b}_k(t + \tau)$. Robustness was assessed by testing the statistical significance of the squared covariance (SC) and the correlation between $\mathbf{b}_k(t + \tau)$ and $\mathbf{a}_k(t)$, using a moving blocks bootstrap approach (von Storch and Zwiers 1999). Each MCA was repeated 100 times, linking the original SST dataset with randomly scrambled Z_{500} ones, so that the chronological order between the two variables was destroyed. Note that only the order of the years was changed, not that of the months (always groups of 3 consecutive months, so that the autocovariance matrix of Z_{500} at lags of 1 and 2 months is unchanged), and the scrambling was applied to groups of 2 consecutive years to further reduce the influence of serial correlation (for instance, 1958–59–60–61 . . .

1997 becomes 1967–68 78–79 . . . 1945–46). The quoted significance levels indicate the percentage of randomized square covariance and correlation for the corresponding mode that exceed the value being tested. They are very robust, as very similar levels of statistical significance were obtained when the MCA approach was altered (e.g., using several ensembles of 100 permutations). Only the first mode of the MCA ($k = 1$) will be discussed, as no significant relation was found in higher modes when the ocean was leading the atmosphere.

3. General description of the MCA results

Lagged covariance is powerful in distinguishing between cause and effect in the extratropical latitudes as on a monthly or longer timescale the atmosphere primarily acts as a white noise forcing on the ocean. If the ocean only responds passively, there should be no covariance when the ocean leads by more than the atmospheric persistence time. Because of this intrinsic atmospheric persistence, the covariance is large when the two media are in phase, but it peaks when the ocean lags if the data are averaged over a duration smaller than the oceanic timescale; otherwise the maximum covariance occurs in phase. At larger lag, the covariance decays like the oceanic anomalies. If SST fluctuations influence an atmospheric variable, their cross covariance does not vanish when the ocean leads, the covariance remaining of the same sign if there is a positive air–sea feedback, but still peaking when the ocean follows (Frankignoul 1985). Such signatures are searched for here by applying a MCA between SST and tropospheric variables as a function of time lag, along the course of a year.

We present in Fig. 1 the SC of the first MCA mode in the analysis with Pan-Atlantic (20°S–70°N) SST and Z_{500} anomalies. The SC has a pronounced seasonal and lag dependence, being the largest in wintertime when the height field leads SST by one month. Figure 2 illustrates the associated patterns for SST (gray shading) and Z_{500} (contours) when the latter is fixed to November–December–January (NDJ) and the SST field lags by 1 month to leads by 7 months. When the height field leads by 1 month or in phase with the SST anomalies, we recover the NAO signature at 500 mb (Wallace and Gutzler 1981), associated with a tripolar SST pattern (Wallace et al. 1990). This association is found throughout the winter, and since the SC is the strongest when the NAO leads the tripole by one month and then decays at longer positive lags (Fig. 1), this reflects that the SST tripole is primarily a response of the ocean mixed layer to the variability of the NAO. The latter acts as a stochastic forcing, primarily through anomalous surface heat exchange, as documented in various studies (e.g., Cayan 1992; Deser and Timlin 1997; CF99). This atmosphere to ocean forcing is thus the zero-order description of the interaction between the NAO and Atlantic SST.

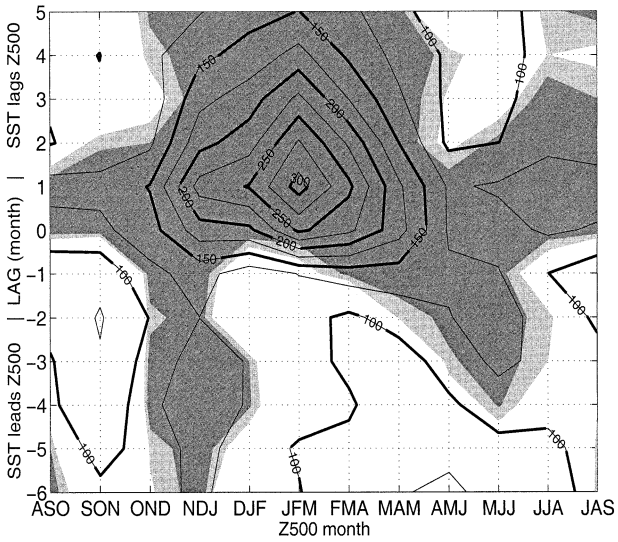

FIG. 1. The SC of the first MCA mode between Pan-Atlantic SST and Z_{500} anomalies (the SCs are dimensionless as the SST and height fields have been normalized—see section 2). SST leads Z_{500} at negative lags indicated (in months) on the *y* axis while the *x* axis denotes the months assigned to Z_{500}. The shaded area indicates where the covariance is statistically significant at the 5% and 10% level (dark and light shading, respectively).

Figure 1 nevertheless indicates that significant covariances (indicated by shadings) are also found when SST leads Z_{500} by several months in two seasons: early winter (NDJ) and late spring (MJJ). As shown in CF99 the late spring Z_{500} anomalies covarying with preceding SST depict an anomalous circulation over the Hudson Bay while the early winter signal strongly resembles the NAO. As seen in Fig. 2 (negative lags) we recover CF99's NAO signature at 500 mb in early winter, and the good correspondence between a reference NAO (taken here as the first EOF of Z_{500} anomalies in winter) and the Z_{500} pattern seen in Fig. 2 in both lead and lag conditions is demonstrated in Fig. 3 and Table 1. Accordingly, we will make no further distinction between the NAO and the height field anomaly found in the MCA. In Fig. 2, the SST pattern preceding the NAO extends throughout the oceanic domain. Preceding a negative NAO phase, there is a warm SST anomaly along the eastern side of the North Atlantic, extending down to about 20°S, so that the same sign is seen north and south of the equator. There is also a cold SST anomaly centered south of Newfoundland near 40°N, plus a well-defined center of action along the equator, which is particularly strong near 10°W at lags −1, −2, and −5. These results are consistent with CF99, who only considered SST anomalies north of 20°N and a different atmospheric dataset. They suggest that tropical SST anomalies are also seen prior to early winter NAO events.

Based on the square of the correlation between the Pan-Atlantic SST and height field pattern found in the MCA at lag −4 (0.53), the associated predictive skill

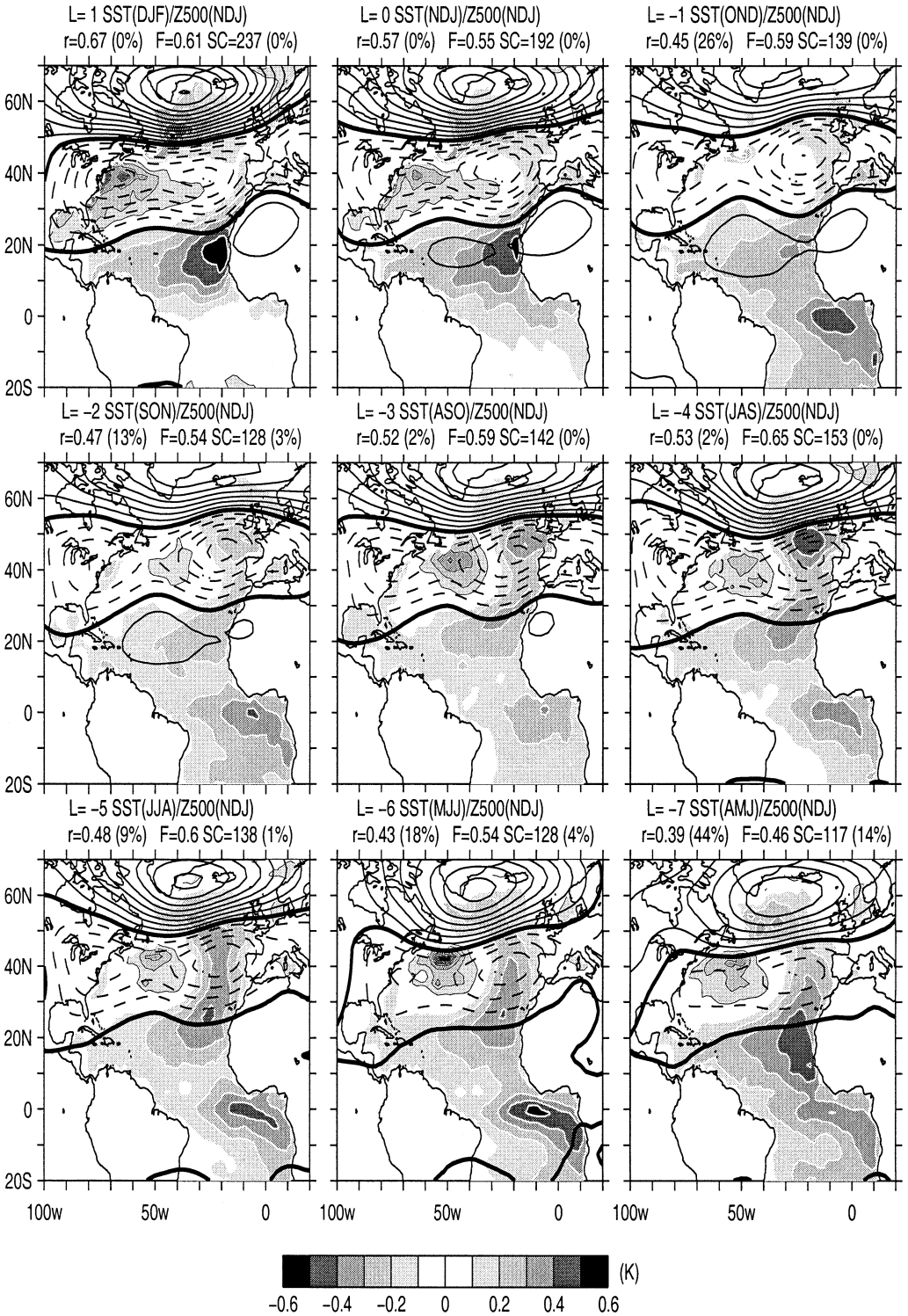

FIG. 2. Heterogeneous Z_{500} (thick contours, CI = 5 m with negative values dashed) and homogeneous SST (gray shading in K with white contours for positive values and black contours for negative values) covariance maps for the first MCA mode between Pan-Atlantic 500-mb height and SST anomalies in early winter (Z_{500} fixed in NDJ, SST lagged as indicated). The results are shown from lag −7 to +1. The correlation coefficient r between the SST and Z_{500} MCA time series, the SC fraction F, and the SC of the mode are given for each lag. The percentages in parentheses for r and SC give their estimated significance level.

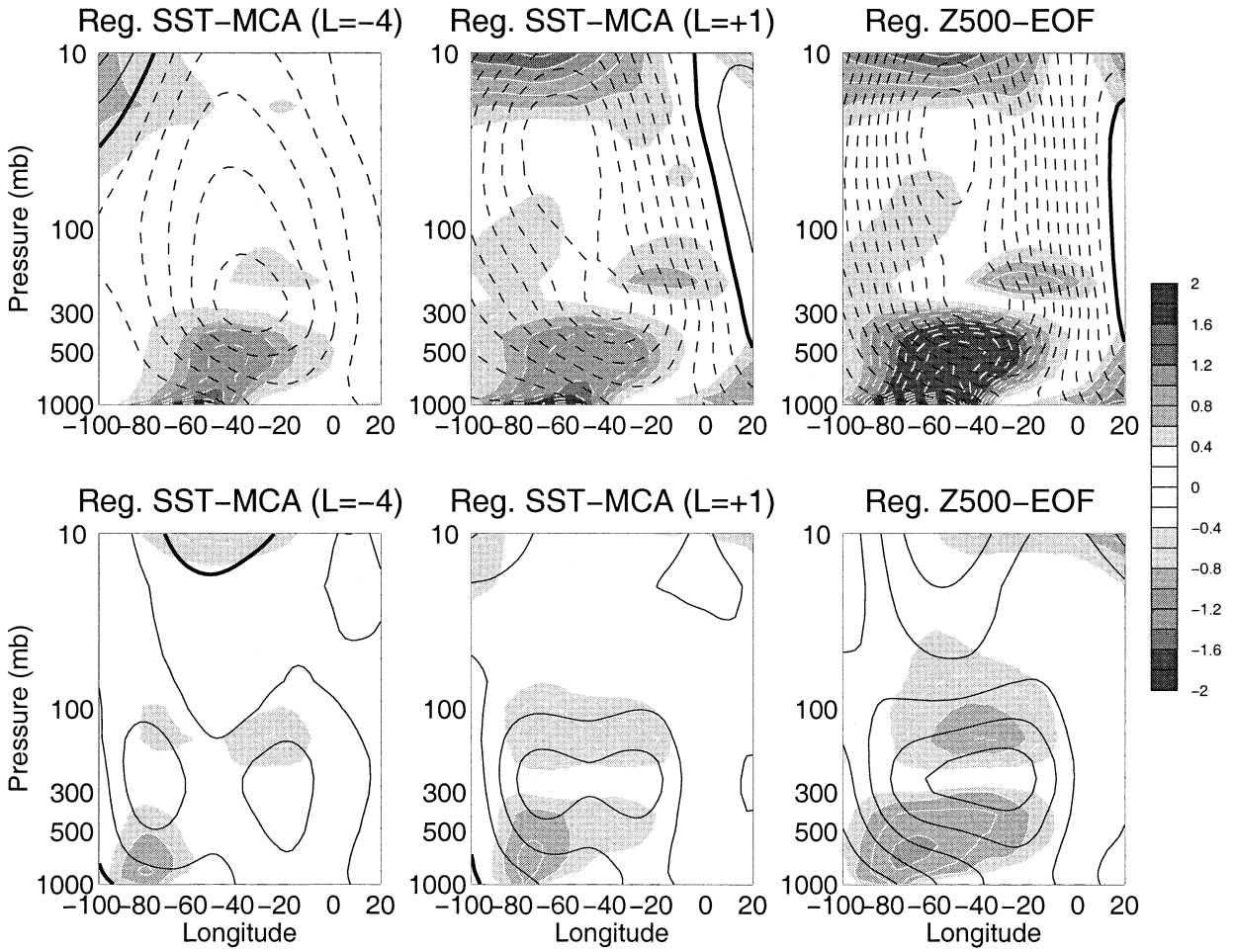

FIG. 3. Height (contoured every 10 m, dashed for negative) and temperature (in K—see the black and white color bar—white dashed for negative) regression maps at (top) 65°N and (bottom) 40°N. The left (middle) panel maps are based on the MCA–SST time series when SST leads (lags) Z_{500} by 4 months (1 month), while the right panel maps are based on an EOF analysis. All regression maps are based on NDJ anomalies.

in the hindcast mode is 27% of the early winter NAO variance, and about half that number in the forecast mode (see section 6). To determine which part of the Pan-Atlantic SST pattern contributes most to the NAO predictability, we have conducted two separate analysis with (i) midlatitude (north of 20°N) SST and Z_{500} (ii) Pan-Atlantic Z_{500} and tropical (20°S–20°N) SST.

TABLE 1. Correlation between the (top) Z_{500} heterogeneous maps and (bottom) time series from the MCA and the NAO, defined as the first EOF of the Z_{500} anomalies in NDJ. The correlations are given for three domains. The numbers without parentheses refer to the MCA at lag +1, and those in parentheses refer to the MCA at lag −4, except for the middle column (tropical SST–Pan-Atlantic Z_{500}), which refers to lag −2.

MCA domain	>20°S SST, Z_{500}	20°S–20°N SST, >20°S Z_{500}	>20°N SST, Z_{500}
Spatial correlation	0.98 (0.95)	0.96 (0.8)	0.98 (0.93)
Temporal correlation	0.98 (0.96)	0.97 (0.87)	0.98 (0.95)

Figure 4 indicates that there are large differences in the structure of the covariance in the two analysis. It suggests that the late spring covariance when SST leads in Fig. 1 originates from the Tropics (Fig. 4b), with little indication of it in the midlatitude analysis (Fig. 4a). The anomalous circulation over the Hudson Bay in late spring is thus mostly related to tropical Atlantic SST anomalies. This will be studied elsewhere. Focusing from now on on the *early winter period*, we see that both analyses show significant SC when SST leads, albeit over longer lead times and during a broader season in the midlatitude case (the SC is only significant in early winter with tropical SST but during the whole cold season with midlatitude SST). We suggest below that the covariability seen at negative lags in Fig. 2 actually reflects two competing oceanic influences on the NAO (one from the midlatitudes, one from the Tropics), with the bulk of the signal coming from the midlatitudes.

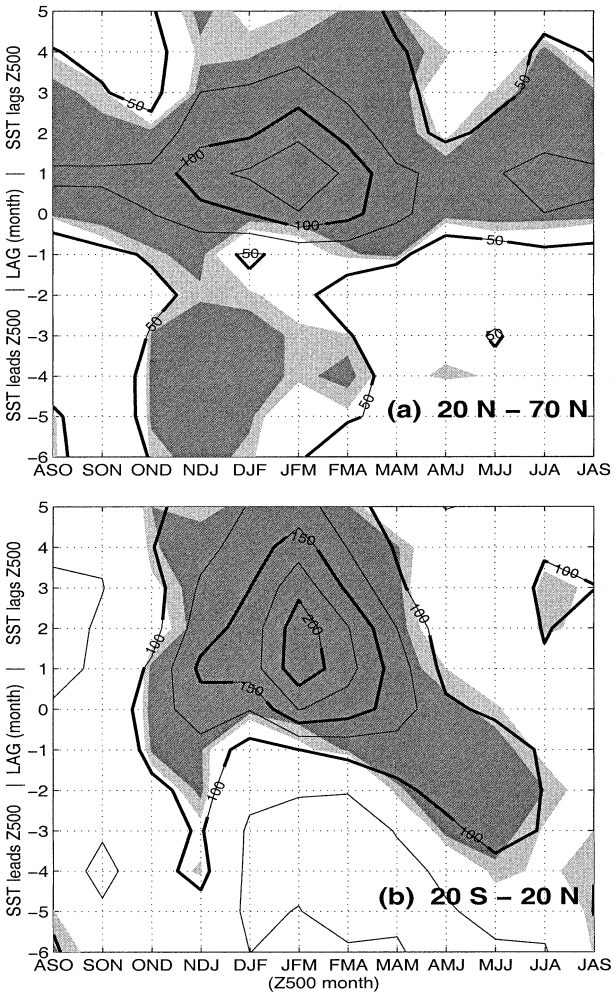

FIG. 4. Same as Fig. 1 but for (a) midlatitude (20°–70°N) SST and Z_{500} anomalies (b) tropical (20°S–20°N) SST and Pan-Atlantic (20°S–70°N) Z_{500} anomalies.

4. Midlatitude SST forcing of the NAO

a. A local impact of North Atlantic SST onto the NAO

The SST and Z_{500} patterns obtained in the midlatitude analysis (Fig. 5) are essentially similar to those found in Fig. 2 north of 20°N, and the Z_{500} pattern seen at negative lags is again highly similar to the NAO (Table 1). A correlation analysis of the MCA–SST time series at lag −4 (Fig. 6, top) with ''global'' SST anomalies (Fig. 6, gray shading) indicates that the SST pattern in Fig. 5 is primarily confined to the Atlantic and limited to latitudes north of about 10°N. The confinement of the SST pattern to the North Atlantic may seem surprising, since Fig. 2 showed a continuous SST pattern from 70°N to 20°S, but it is consistent with the presence of two distinct oceanic influences on the NAO, one from the midlatitudes and one from the Tropics, which are mixed in Fig. 2. We shall refer to the SST pattern in Fig. 6 as the North Atlantic horseshoe pattern (NAH). We show in appendix B that the NAH pattern primarily results from local atmosphere–ocean interactions during the warm season, but also partly reflects the winter to summer evolution of the SST tripole (see section 4c).

The global correlation map between Z_{500} and the MCA–SST time series at lag −4 (Fig. 6, contour) shows that the NAH influence at 500 mb is similarly restricted to the North Atlantic sector, with stronger correlations over Greenland than over the Azores (respectively, 0.4 and 0.3). Clearly, a substantial fraction of the NAO signal seen in Fig. 2 reflects extratropical atmosphere–ocean interactions over the North Atlantic.

The relationship between the wintertime NAO and NAH several months earlier is so strong that it is also found implicitly in the SST anomaly field alone. Using the correlation of the SST anomaly field in successive 3-month periods with the NAH time series (again using lag −4 for its definition), Fig. 7 represents (somewhat noisily) the time evolution of the NAH pattern. At small lags, the correlation map primarily reflects the SST anomaly persistence, but around NDJ there is a rapid transformation of the NAH pattern into the SST tripole. The transition between summer and winter patterns, with the development of a negative SST anomaly at the western boundary, is opposite to what would be expected from mean current advection, and it cannot be explained either by the progressive deepening of the mixed layer, except perhaps for the loss of correlation near 40°N–50°W. However, the correlation maps can be explained by the influence of the NAH anomaly pattern onto the atmosphere: the NAH generates a NAO response, which in turn generates a SST anomaly tripole. In this scenario, the NAO acts as an ''atmospheric bridge.''

The relationship between NAH and the NAO is also found when the MCA between SST and Z_{500} is based on all the calendar months, albeit with a reduced significance level (Fig. 8). As in the two previous MCA (Figs. 2 and 5), we observe in Fig. 8 a drop in significance at lag −1 and −2. We suggest below that this is due to the competing influence of the Tropics on the NAO, and possibly also to intrinsic atmospheric persistence at lag −1.

b. Orders of magnitude

The MCA in Fig. 5 revealed a significant and robust covariance between the NAH pattern and the winter NAO when NAH leads the NAO by up to 6 months. To verify that a covariance on such a long lead time can result from the long persistence of the NAH anomaly, provided that it indeed forces a NAO-like signal, let us assume that the time evolution of the NAO, described by Z, may be linearly decomposed into a stochastic component F and an SST-induced signal fT

$$Z(t) = F(t) + fT(t - \delta), \tag{3}$$

where f measures the strength of the NAH forcing and

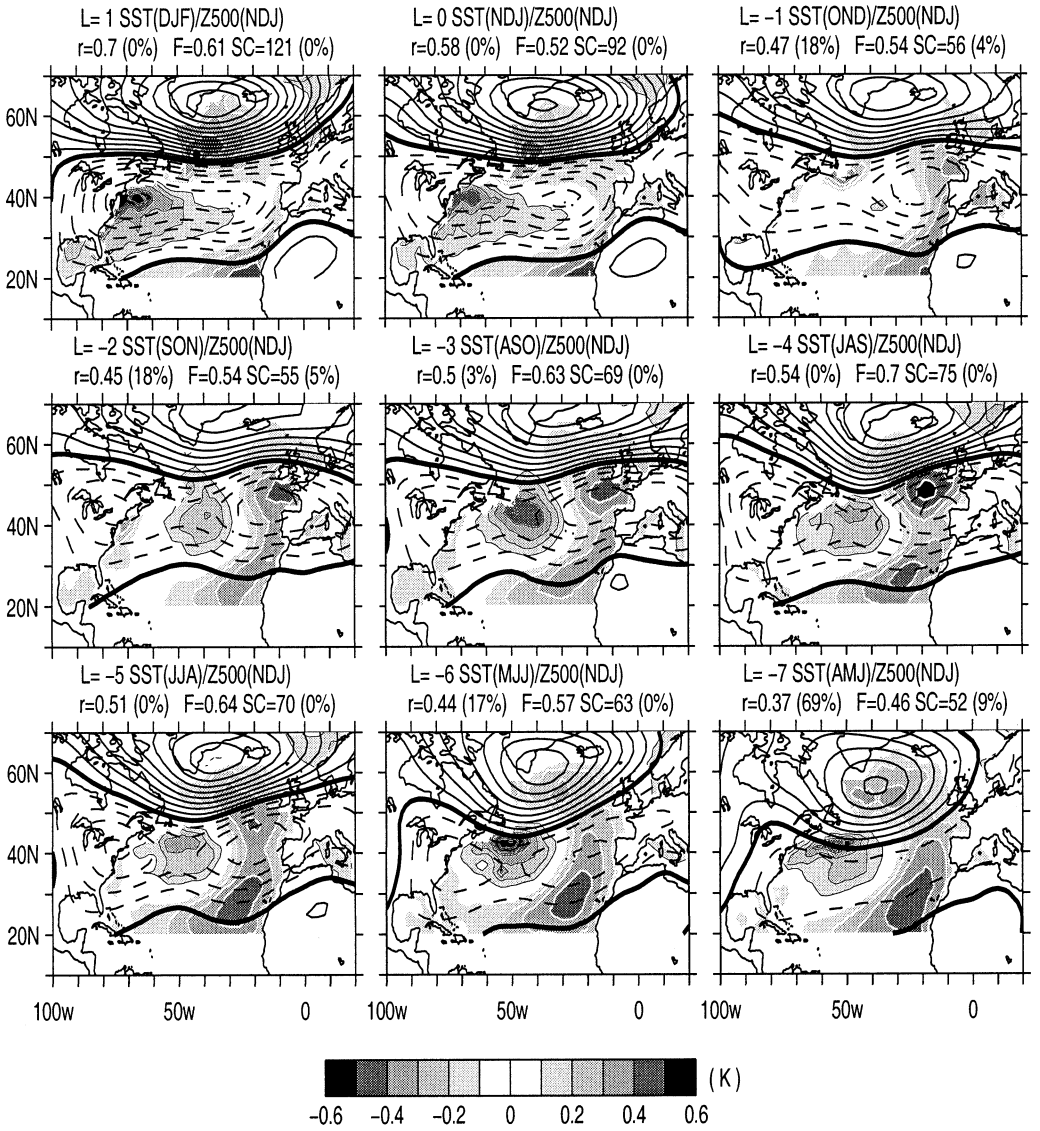

FIG. 5. As in Fig. 2 but for the first MCA mode between midlatitude (20°–70°N) SST and Z_{500} anomalies.

δ denotes the (short) atmospheric adjustment time to SST changes. During winter, the NAO is rather persistent, resulting in a significant autocorrelation at 1-month lag, in particular when the NAO is most energetic (Table 2). Let us assume that this month-to-month persistence primarily reflects intrinsic atmospheric dynamics, and that F is essentially decorrelated at lags longer than 1 month. Multiplying (3) by $T(t - \tau)$ and taking an ensemble average (denoted by a bracket), we have

$$\langle Z(t)T(t - \tau)\rangle \simeq f\langle T(t - \delta)T(t - \tau)\rangle \quad \text{for } \tau \geq 2 \text{ months} \qquad (4)$$

so that the covariance when T leads Z by τ months simply depends on the SST autocorrelation at lag $\tau - \delta$. If the SST persistence is sufficiently large and its impact on the NAO important (large f), a significant covariance is expected at long lead times, and it should *not be interpreted* as a τ-month delayed response of the atmosphere to NAH. Instead, it reflects that there is a rapid adjustment of the atmosphere to NAH (measured by δ), and that NAH *is persistent*. For a given SST persistence, the stronger the SST forcing, the longer the lag at which a significant covariance can be detected. Note that this is essentially independent of the atmospheric adjustment time δ, if it is indeed short, and of the NAO intrinsic persistence, if τ is large enough for (4) to be satisfied.

The persistence of the NAH pattern is about 4.5 months [the autocorrelation of the lag −4 NAH time series is well approximated by an exponential decay, as in the in the Frankignoul and Hasselmann (1977) model]. With significant covariances between NAH and

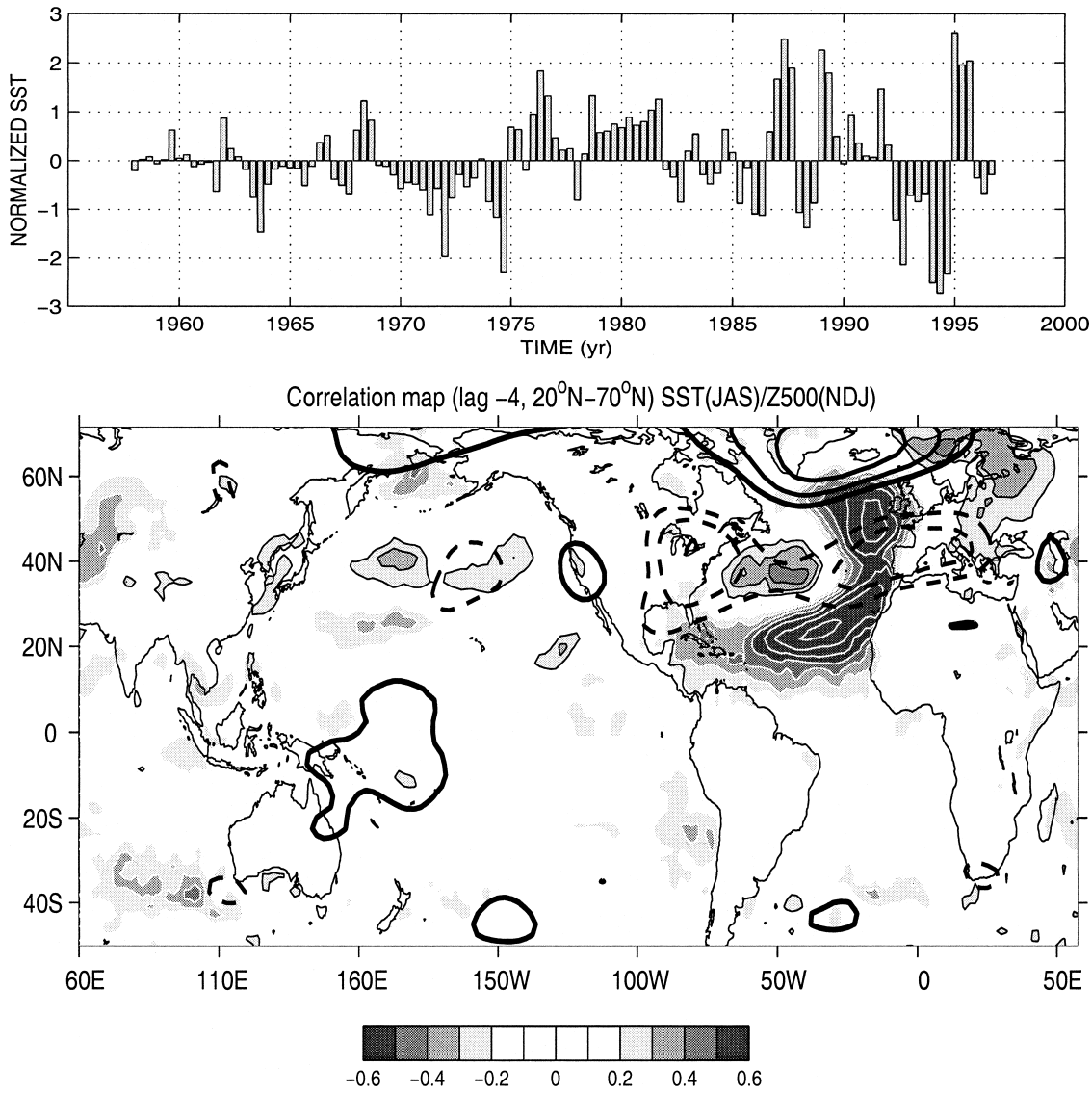

FIG. 6. (top) Normalized SST time series obtained from the MCA between midlatitude (20°–70°N) SST and Z_{500} at lag −4 (Fig. 5). Each year consists of three vertical bars (Jul–Aug–Sep). When positive, it indicates a warming of the North Atlantic subtropics. (bottom) Correlation maps of Z_{500} (thick black contours, CI = 0.1) and SST (same convention as in Fig. 2) onto the above SST time series. Only correlations with amplitude $\geq$0.2 are indicated, with increments of 0.1.

the NAO when the former leads by up to 6 months, the MCA in Fig. 5 is thus consistent with Eq. (3) and a strong oceanic forcing. The latter can be estimated as follows. At lags −3 and −4, the SST anomaly is typically 0.35 K and the Z_{500} perturbation is 40 m over Iceland (Fig. 5). In 3 months, the NAH amplitude decreases by a factor of 2. Hence, if the atmospheric adjustment time can be neglected, the instantaneous association between NAH and the height anomaly over Iceland at 500 mb is 40 m for $0.35/0.5 \simeq 0.7$ K, which amounts to a forcing $f = 57$ m K^{-1} at 500 mb. A similar reasoning applied to lag −4 yields a weaker figure of 36 m K^{-1}, so that a rough estimate is $f = (57 + 36)/2 \simeq 45$ m K^{-1}, that is, a height anomaly of 45 m over Iceland for a NAH anomaly of 1 K (the latter denoting the amplitude at the centers of action of the NAH pattern). The impact over the Azores is weaker by about a factor of 2 (the height perturbation is 20 m), consistent with the asymmetry of the NAO pattern at 500 mb (see Fig. 5). For both regions, this is certainly an overestimation because of the maximization inherent to the MCA. However, note that even larger figures would be obtained if the atmospheric adjustment time δ was not neglected in (4).

Equation (4) predicts that unless δ is very large the covariance should keep increasing as the lag decreases, until the autocorrelation of the intrinsic part of the forcing, F in (3), becomes significant, that is, the lag −1.

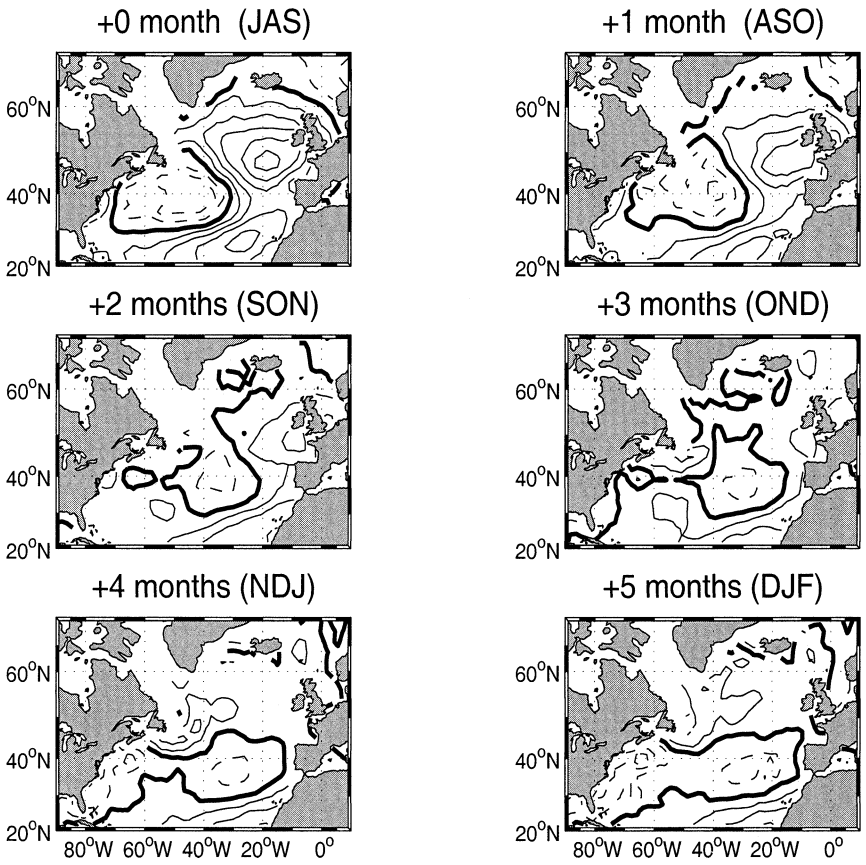

FIG. 7. Lagged (in months, as indicated on the plot) regression maps of SST anomalies (every 0.1 K, dashed for negative, zero contour thickened) onto the normalized MCA–SST time series shown in Fig. 6 (top).

This cannot explain the decrease of covariance and significance systematically seen in the previous MCAs at lag −2 (Figs. 2, 5, 8). It is argued below that the decrease results from the competing influence of an essentially uncorrelated remote forcing of the NAO from the Tropics.

c. *A positive feedback between the SST tripole and the NAO*

The NAH and SST tripole patterns are compared in Fig. 9, where the SST tripole (gray shading) is a regression map of late winter (FMA) SST anomaly onto the MCA–SST time series at lag +1 (Z_{500} fixed in JFM), and the NAH pattern (contour) is reproduced from Fig. 5 (lag −4). The patterns share common features, and their spatial correlation is 0.57. In both cases the SST anomaly reduces the meridional SST gradient along 40°N and enhances it along 25°N, for the polarity in Fig. 9. The NAH pattern is however more confined meridionally than the tripole, and shifted to the northeast.

As NAH impacts the NAO, by projection the tripole also forces the NAO, the signs being such as to provide a positive feedback. Using the spatial correlation between NAH and the tripole, the strength of the positive feedback is estimated to be $0.57 \times 45 \simeq 25$ m K^{-1}.

The connection between the tripole and the NAH pattern might be more subtle. The tripole reaches its maximum amplitude in late winter–spring as a result of the NAO forcing. It is then distorted by advection, which should make it resemble more the NAH pattern, while being slowly damped, primarily via the negative heat flux feedback (Frankignoul et al. 1998). The tripole should thus contribute to the NAH amplitude in summer and fall (explaining about 40% of the NAH amplitude during that time, see appendix B), and may be more actively involved in the forcing of the NAO than is directly implied by its projection onto the NAH pattern. The chain of arguments is again indicative of a positive feedback between the tripole and the NAO.

5. Tropical SST forcing of the NAO

In the MCA between tropical Atlantic SST anomalies (20°S–20°N) and Pan-Atlantic 500-mb height anomalies (Fig. 10), the tropical SST patterns are close to those found in Fig. 2. At positive or zero lags, the anomalous SST maximum is located between 10° and 20°N, re-

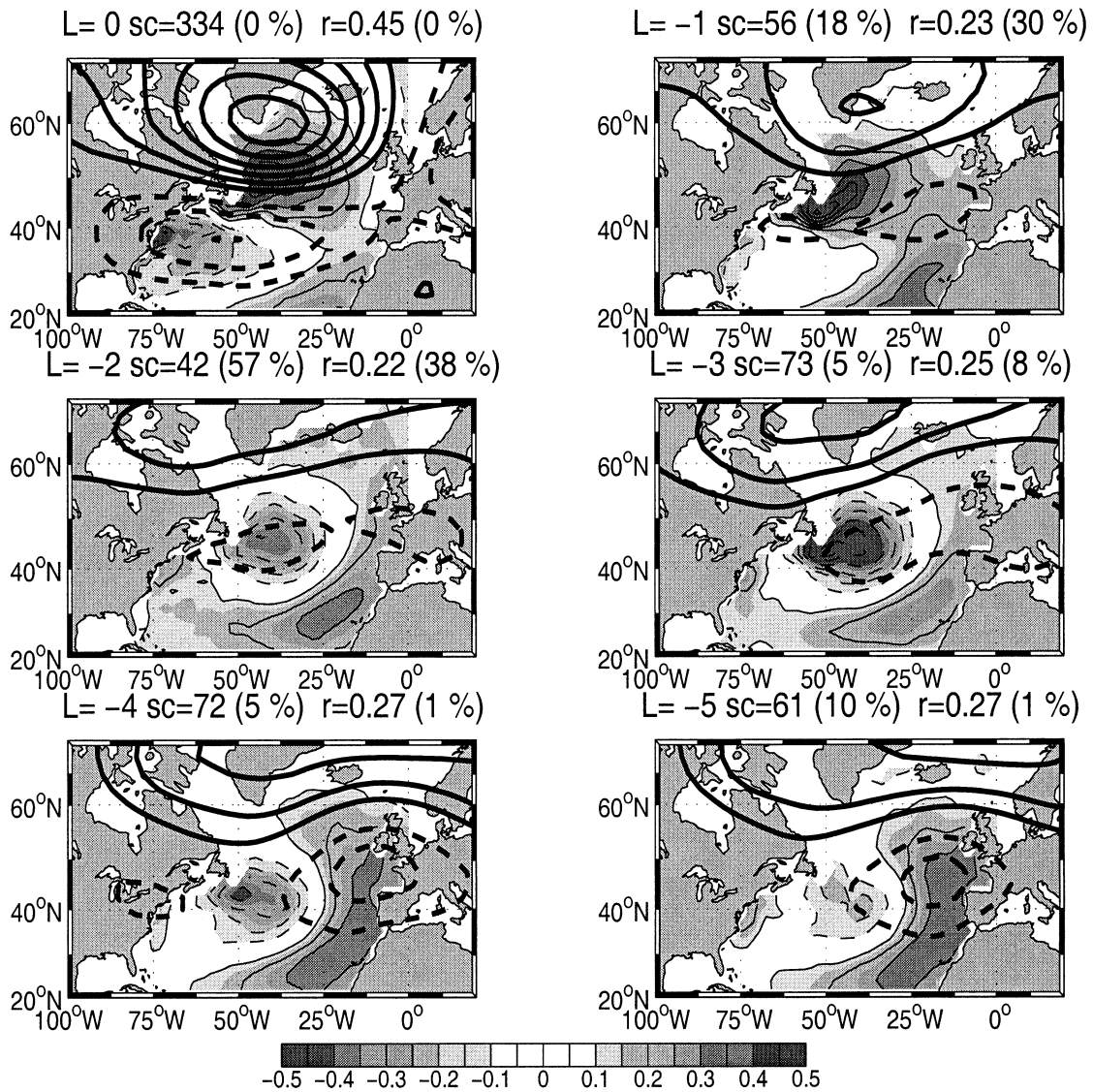

FIG. 8. Same as Fig. 5 but considering all calendar months. The SST anomaly (gray shading) is contoured every 0.1 K (dashed for negative). The Z_{500} is contoured every 5 m (dashed for negative).

flecting the southern lobe of the SST tripole forced by the NAO. When SST leads by 1–3 months, the center of action is centered on the equator, near 10°W, and the amplitude is substantial in the eastern part of the basin between 10°S and 5°N. A warming of the tropical Atlantic thus precedes by 1–2 months a dipolar height anomaly at higher latitudes, reminiscent of a negative NAO phase. Again, since the analysis is linear, a cooling of the surface tropical Atlantic precedes by a couple of month an opposite sign dipolar height anomaly. The Z_{500} pattern when SST leads is overall similar to that found in Fig. 2, but the height anomalies are more symmetric north and south of 50°N than they are at zero lag. This is reflected in the weaker spatial and temporal correlation with the NAO than found in the midlatitudes analysis (see Table 1). Nevertheless, the correlations remain strong enough to make no further distinction with the NAO.

There are two important differences in this analysis compared to that with the midlatitude SST in section

TABLE 2. Amplitude (in m, computed as in Fig. B1) and 1-month autocorrelation $r(1)$ of the first PC of Z_{500} monthly anomalies over the North Atlantic sector (20°–80°N, 100°W–20°E) for various groups of three successive months. The associated spatial pattern (first EOF) is taken as a reference NAO at 500 mb. Bold characters indicate that $r(1)$ is significantly different from zero at the 5% level, assuming independent samples.

Season	OND	NDJ	DJF	JFM	FMA	MAM
$r(1)$	0.14	**0.25**	**0.22**	**0.28**	**0.24**	−0.01
Amplitude	38	45	49	51	46	38

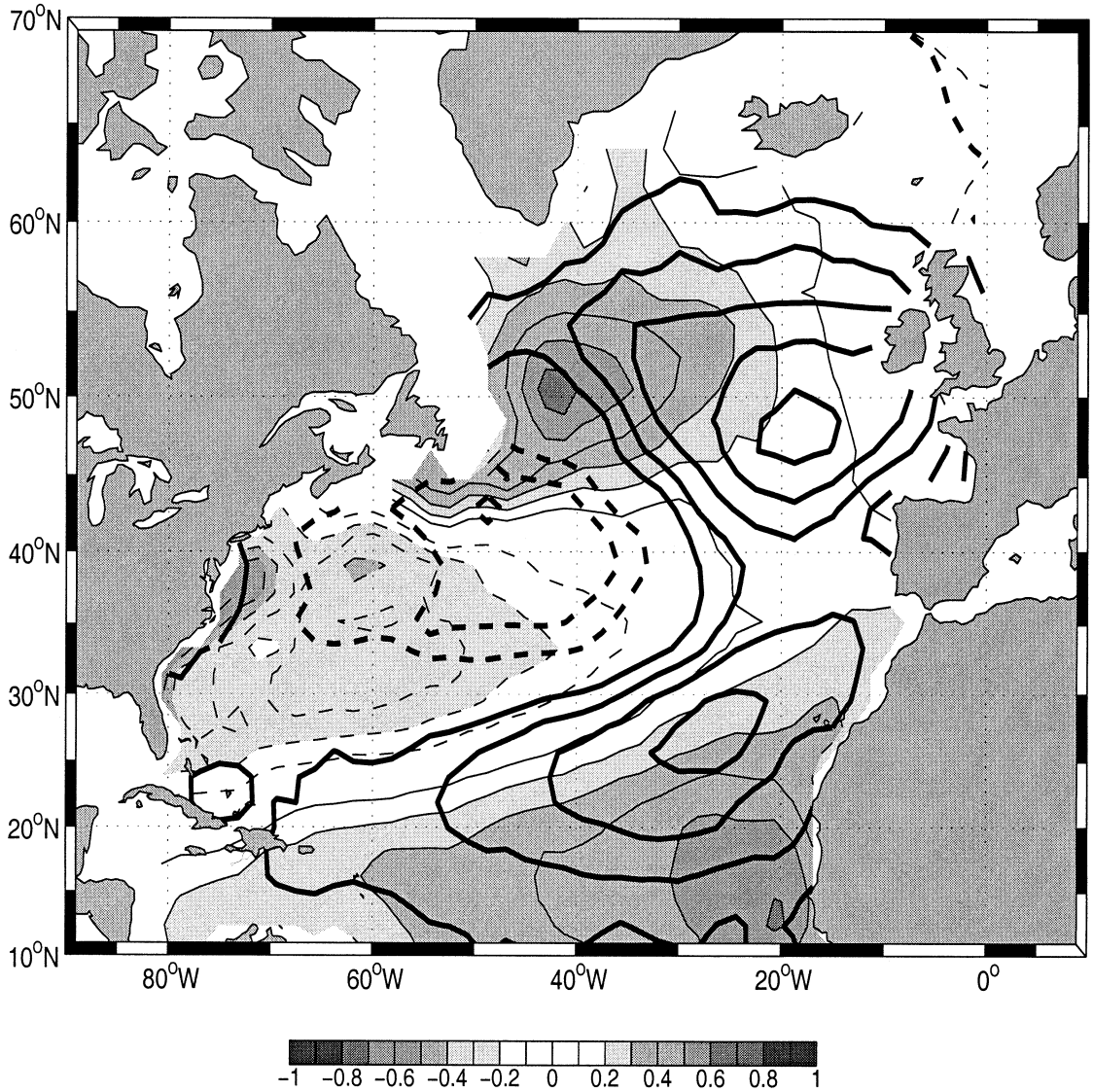

FIG. 9. SST regression maps showing the tripole (in K, gray shading, dashed contours for negative) and the NAH patterns (thick contours, every 0.1 K, dashed for negative).

4a (cf. Figs. 4a and 4b when Z_{500} is fixed in wintertime). (i) a significant covariance when tropical SST leads the NAO is only found at short lead time (1 and 2 months), whereas it was found for up to 6 months with midlatitudes SST anomalies, which suggests a weaker SST impact on the NAO. (ii) The covariance when SST leads is only significant in early winter (NDJ), whereas it was significant from October–March in the midlatitude case. This suggests that the tropical SST forcing is more sensitive to the seasonal cycle and only occurs in early winter.

a. The tropical Atlantic SST and the NAO

To determine the meridional extent of the tropical Atlantic warming seen at negative lags in Fig. 10, we show in Fig. 11 (top, gray shading) the simultaneous correlation of the MCA–SST time series at lag −2 with Atlantic SST anomaly. Consistent with Fig. 6 (gray shading), which showed weak correlation of the NAH pattern with the tropical SST, the correlation map indicates that the tropical SST signal does not penetrate to a higher latitude than about 20°N. So, we can think that to a good approximation, the two SST patterns (NAH and the tropical warming/cooling) are essentially unrelated. A physical interpretation is that these SST patterns have very different origins. As demonstrated in appendix B, the NAH pattern reflects largely the summer to fall extratropical air–sea interactions, while the tropical SST pattern is highly reminiscent of the Atlantic Niño mode of Zebiak (1993), and may be thought of as an intrinsic atmosphere–ocean coupled mode over the

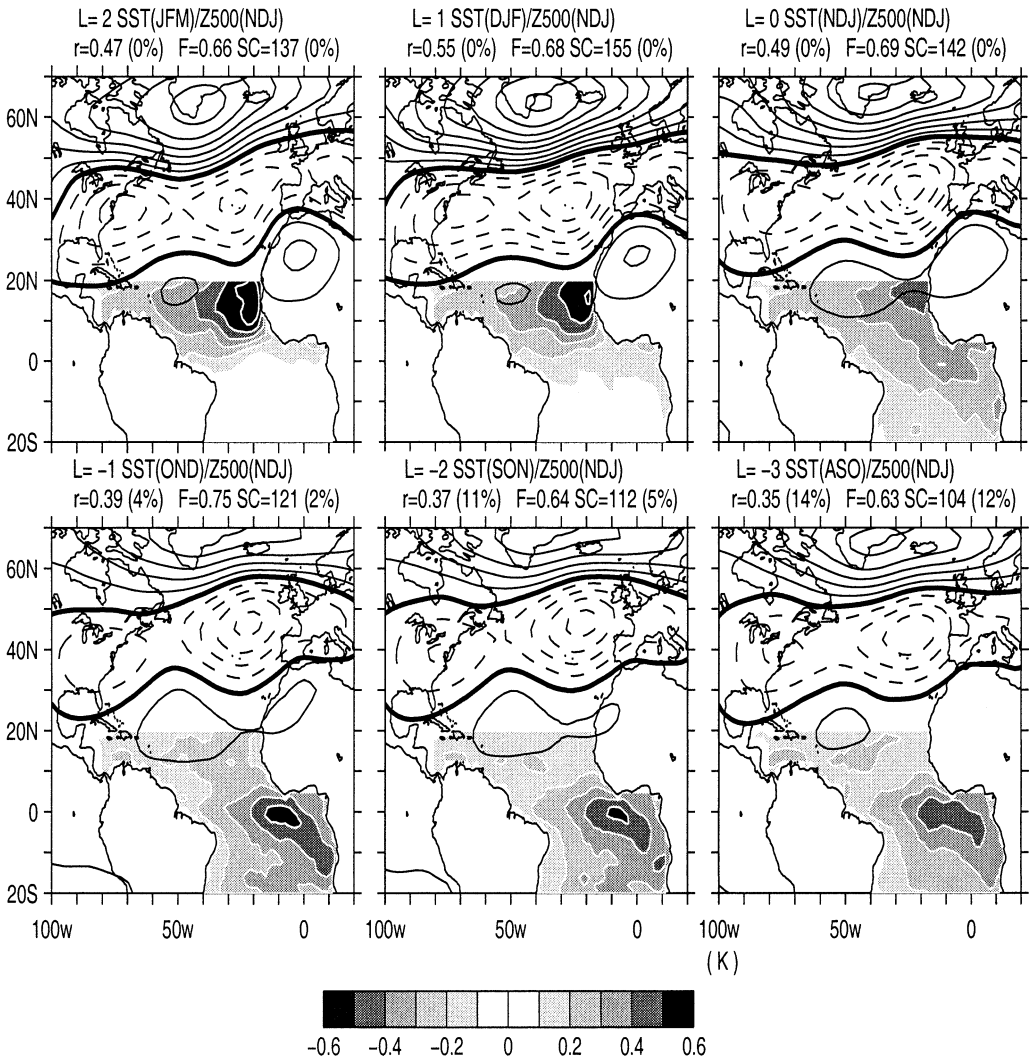

FIG. 10. As in Fig. 2 but for the first MCA mode between Pan-Atlantic Z_{500} (20°S–70°N) and tropical (20°S–20°N) SST anomalies.

tropical Atlantic; the correlation coefficient between the MCA–SST time series at lag −2 and Zebiak's ATL3 SST index (averaged SST over 3°S–3°N, 20°W–0°) is 0.86.

To document the atmospheric circulation anomalies that follow the tropical Atlantic warming, Fig. 11 (top, arrows) shows the correlation of the MCA–SST time series at lag −2 with surface winds 2 months later. A cross-equatorial southward wind is associated with the warm SST in the equatorial band, with some indication of a convergence in midbasin, just south of the equator. A northward wind anomaly is also found near 20°S, so that overall there is a surface convergence over and to the south of the warm SST. This surface wind pattern is broadly consistent with that displayed by Zebiak (1993). Similar correlation maps for the surface turbulent heat flux (latent + sensible) anomalies indicate heating of the atmosphere over the warm SST (not shown), so that the tropical atmosphere seems to respond directly to the SST forcing. In the Northern Hemisphere, the anomalous surface circulation is cyclonic, resulting in reduced (increased) westerlies along 55°N (40°N), and thus a negative NAO phase.

The connection between the local atmospheric response to a warm tropical SST and the remote NAO signal is nicely seen in the correlation map for the 200-mb zonal wind (Fig. 11, bottom), where anomalous easterlies in the deep Tropics (15°S–15°N), west of the strongest SST warming, are flanked to the north and south by anomalous westerlies and thus an enhanced subtropical jet along the 30° parallels. Although of much weaker amplitude and smaller spatial extent, it is reminiscent of the anomalous atmospheric circulation found during warm ENSO events (Horel and Wallace 1981).

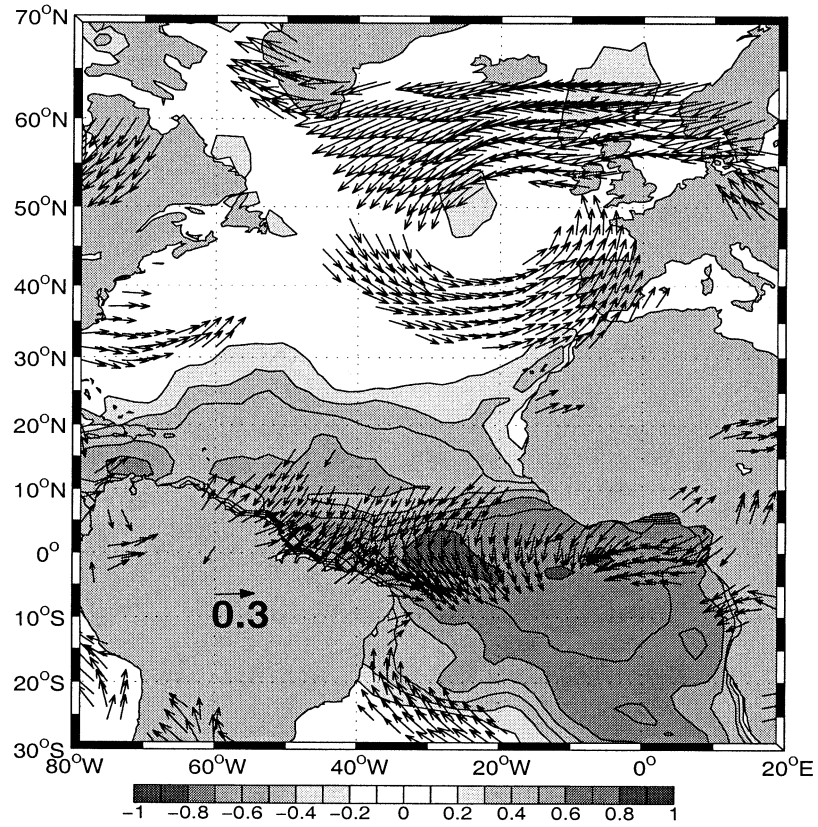
70°N
60°N
50°N
40°N
30°N
20°N
10°N
0°
10°S
20°S
30°S
80°W
60°W
40°W
20°W
0°
20°E
0.3
−1 −0.8 −0.6 −0.4 −0.2 0 0.2 0.4 0.6 0.8 1

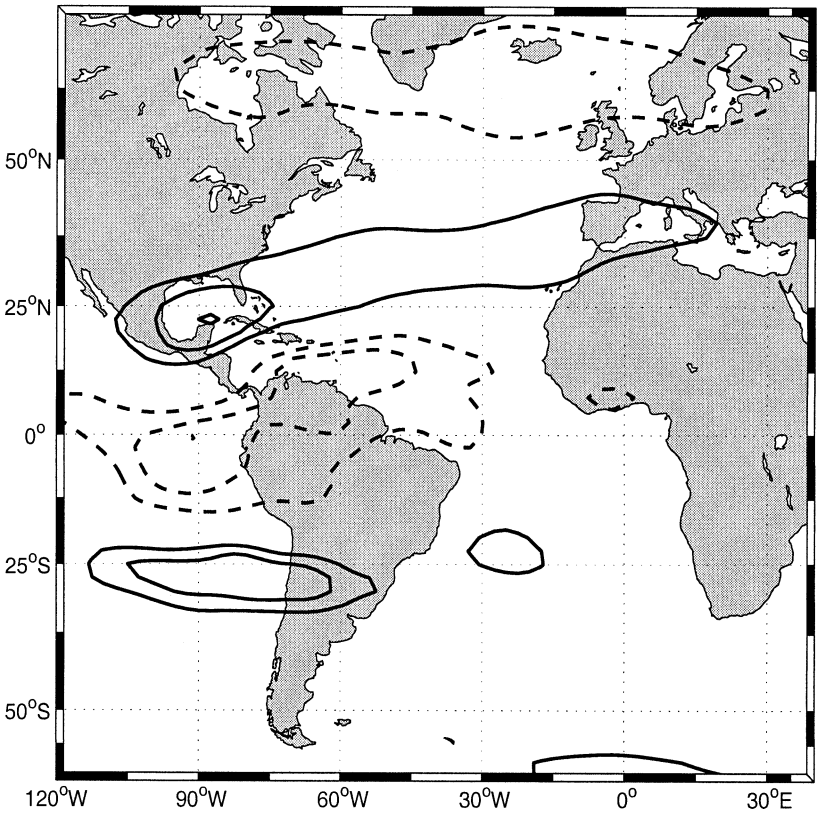
50°N
25°N
0°
25°S
50°S
120°W
90°W
60°W
30°W
0°
30°E

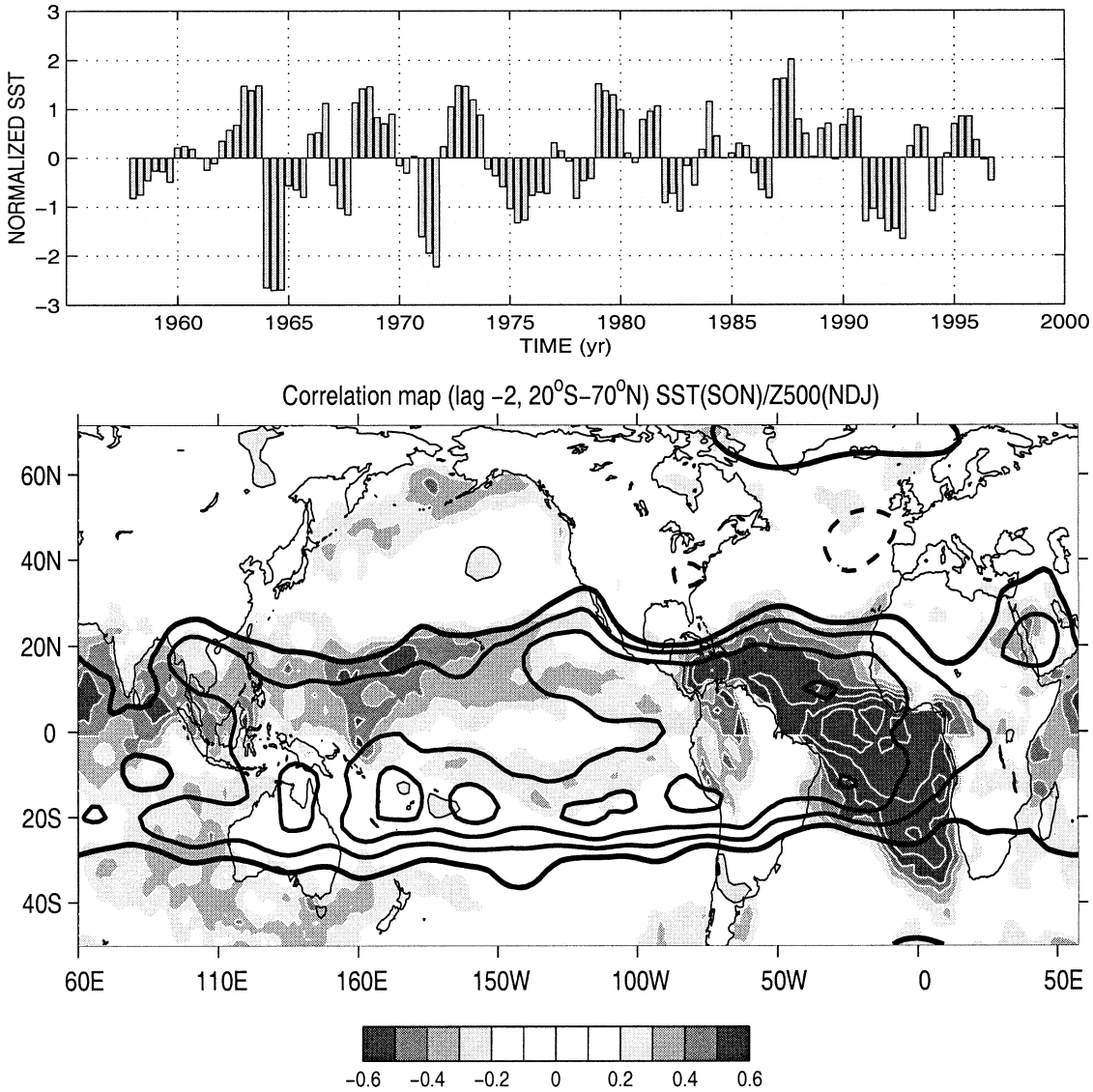

FIG. 12. (top) Normalized SST time series obtained from the MCA analysis between tropical-Atlantic SST (20°S–20°N) and Pan-Atlantic Z_{500} (20°–70°N) at lag −2 (Fig. 10). Each year consists of three vertical bars (Sep–Oct–Nov). When positive, it indicates a warming of the tropical Atlantic. (bottom) Correlation maps of Z_{500} (thick black contours, CI = 0.1) and SST (same convention as in Fig. 2) onto the SST time series above. Only correlations with amplitude ≥0.2 are indicated.

There is also a reduction of the westerlies along 60°N, slightly north of that found at the surface in Fig. 11 (top).

b. Connections to other tropical regions

As shown by Fig. 12, the interaction between the tropical SST pattern and the atmosphere is not limited to the Atlantic basin but is part of a larger-scale phenomenon. The (simultaneous) correlation map (bottom) between SST anomalies in SON and the MCA–SST time series at lag −2 (top) indicates indeed that the SST anomaly is substantial in the Atlantic between 20°N and 40°S, although extending the MCA analysis southward strongly degrades the statistical significance at negative lags (not shown). The SST anomaly also extends over

←

FIG. 11. (top) Correlation maps between SST (gray shading, continuous contours for positive), surface wind stress (arrows) and the MCA–SST time series at lag −2. Only correlation vectors with norm larger than 0.2 are shown. The correlation is simultaneous for SST (SON) but lagged by 2 months for the surface wind stress (taken in NDJ). (bottom) Same as (top) but for the zonal wind at 200 mb (in NDJ), contoured every 0.1 (starting at ±0.2 and dashed for westward wind anomaly).

the Indian and Pacific Oceans in the 0°–20°N belt (gray shading), albeit with a weaker amplitude. The Z_{500} signal (contour, lagging by 2 months the tropical SST time series) is strong throughout the equatorial belt, with correlations reaching 0.5 over the Atlantic and along 20°S in the Pacific. Note that the NAO only appears weakly in Fig. 12. This suggests that the link to the NAO is rather weak, or at least degraded by the competing (and essentially decorrelated) influence from the midlatitude SST forcing.

c. Order of magnitude

Based on the MCA–SST time series, the persistence of the tropical Atlantic SST anomaly is about 12 months, again approximating its autocorrelation function by an exponential, as in the Frankignoul and Hasselmann (1977) model. At both lag -1 and lag -2, Fig. 10 indicates that a 15-m height anomaly over Iceland and the Azores at 500 mb is associated with a 0.4-K SST anomaly in the Tropics. Correcting for the SST anomaly decay in 1 month, its instantaneous association with Z_{500} is 15 m for $\simeq$0.42 K (or based on lag -2, 15 m for $\simeq$0.47 K), yielding an average forcing 30 m K^{-1} at 500 mb. Since the tropical SST forcing yields a symmetric dipolar response at high latitudes, the 30 m K^{-1} sensitivity applies to both Iceland and the Azores regions.

6. Implication for NAO predictability on monthly timescales

Both the NAH and tropical SST influence on the NAO are associated with a predictive skill. Based on the square of the correlation coefficient between the SST and Z_{500} patterns when SST leads, the predictability of the monthly NAO variance in the hincast mode is about 25%, based on the Pan-Atlantic SST or the NAH patterns at lag -4 (correlation of 0.54), and 15% based on the tropical SST pattern at lag -2 (correlation of 0.37). However, as emphasized previously, the lag correlations in the MCA are biased toward higher values. To correct for this bias, we have cross-validated the results by removing successive sets of 3 yr before performing the MCA and then using the MCA patterns to determine the amplitude of the middle year that was removed. Table 3 gives the lag correlations for the cross-validated time series at various lead times. As expected, all correlations decrease, but we now have an estimate of the actual forecast (not hindcast) skill of the NAO associated with its interaction with Atlantic SST on monthly timescales. It is seen from Table 3 that the NAH pattern yields the strongest skill, with a correlation of 0.40 at 4-month lead times, that is, allowing a prediction of 16% of the NAO variance 4 months in advance. The impact of the tropical Atlantic SST goes from 15% (hindcast) to a small 4%, as obtained by squaring the 0.22 and 0.18 correlation at short lead times. The skill obtained with the Pan-Atlantic SST pattern lies between that inferred from the midlatitude and the tropical analysis. See also Rodwell and Folland (2001) for the predictability of the midlatitude case.

7. Discussion and conclusions

Using a maximum covariance analysis (MCA), we have investigated the existence of a lagged covariance between SST and tropospheric anomalies in the NCEP–NCAR reanalysis. We found a robust and highly significant association between a large-scale Pan-Atlantic SST pattern and the early winter NAO when the SST pattern leads the NAO by up to 6 months. This relation is found when using height anomalies at 500 mb but also other variables like sea level pressure, surface winds, and air temperature, often with comparable significance. Although causality is not necessarily implied by this statistical relation, it is consistent with an impact of the Pan-Atlantic SST pattern onto the NAO, and we showed that such long lead times might indeed arise if the NAO responds almost instantaneously to persistent Atlantic SST anomalies. Our analysis suggests that the Pan-Atlantic pattern reflects two competing influences on the early winter NAO.

The strongest influence results from the North Atlantic, primarily poleward of 10°N. The forcing SST pattern for a positive NAO phase has the shape of a horseshoe over the North Atlantic (NAH), with a positive SST anomaly southeast of Newfoundland along 40°N and a negative SST anomaly to the northeast and southeast. This SST configuration precedes a positive NAO phase for several months. An admitedly rough estimate of the strength of the NAO forcing at 500 mb by the NAH pattern suggests 45 m K^{-1}. This is an upper bound because of the maximization inherent to the technique used here, but it is much larger than most AGCM responses to prescribed extratropical SST anomalies (more in the 10–20 m K^{-1} range, as reviewed by Robinson 2000). Our results thus suggest that most AGCMs underestimate the strength of the SST forcing.

The mechanisms behind the midlatitude SST influence are complex. We have interpreted the NAO signal in the lagged MCA as reflecting a rapid (probably about a week) adjustment of the atmosphere to the NAH pattern. In winter, when the NAO is most energetic, the amplitude of the NAH pattern is largely explained by that of the SST tripole, which is the oceanic response to the NAO forcing. So our results suggest a positive feedback between the NAO and the SST tripole, whose strength was estimated to be about 25 m K^{-1} at 500 mb (equivalently $\simeq$2–3 mb K^{-1} at sea level). This feedback is in agreement with recent AGCM simulations (e.g., Rodwell et al. 1999; Watanabe and Kimoto 2000), and it should enhance the NAO variance at interannual and longer timescales, perhaps contributing significantly to the decadal variability of the SST tripole (Deser and Blackmon 1993; Czaja and Marshall 2001). An alternative scenario is that the NAH pattern, which is mostly

TABLE 3. Correlation between the cross-validated SST and Z_{500} MCA time series when SST leads and Z_{500} is fixed to NDJ. The number in parentheses refers to the correlation based on the original MCA time series.

MCA domain (SST pattern)	>20°S SST, Z_{500} (Pan-Atlantic)	20°S–20°N SST, >20°S Z_{500} (Tropical Atlantic)	>20°N SST, Z_{500} (NAH pattern)
Lag-1	—	0.22 (0.39)	—
Lag-2	—	0.18 (0.37)	—
Lag-3	0.33 (0.52)	—	0.35 (0.5)
Lag-4	0.36 (0.53)	—	0.4 (0.54)
Lag-5	0.25 (0.48)	—	0.33 (0.51)

energetic in the warm season, cannot generate an NAO signal at that time for some dynamical reasons (possibly the state of the background atmospheric flow). Nevertheless, as it persists significantly from summer to early winter, it then impacts more efficiently the NAO (possibly because of a more favorable mean atmospheric flow). The two scenario are possible and differ mostly in that the first views the enhanced NAO variability as a result of a constructive interaction with the ocean (positive feedback NAO–tripole), while the second views it as a result of an external forcing (remnant of summer SST anomalies). More observational and modeling studies are needed to clarify this issue.

The tropical Atlantic has a weaker but significant impact on the NAO. It is found that warmer tropical SST precede a negative NAO phase by 1–2 months, with a forcing of about 30 m K^{-1} at 500 mb. The SST anomaly is centered on the equator, extending farther to the south than the north and is related to the Atlantic Niño mode of Zebiak (1993). The tropical Atlantic warming/cooling extends, albeit with a weaker amplitude, in the tropical and in the Indian Ocean, while the atmospheric circulation anomalies found over the tropical Atlantic remain strong throughout the tropical belt. More work is needed to elucidate the nature of this large-scale signal.

In summary, our results indicate that extratropical SST anomalies in the North Atlantic influence more efficiently the NAO than tropical SST anomalies. They are also more pervasive as their impact could be detected during the whole cold season whereas the tropical influence is only seen in early winter. However, the NAH influence remains limited on monthly timescales, and the intrinsic atmospheric variability of the NAO is so strong that only 16% of the total NAO variance was found to be predictable 4 months in advance (actual forecast skill based on cross validated time series). We emphasize that this is the largest forecast skill of the NAO that we could detect in the reanalysis; that associated with the tropical SST was below 5% of NAO variance at a lead time of 1–2 months. Whether AGCMs will be able to reproduce the NAO response that we have detected is at present unclear, but it needs to be investigated.

Acknowledgments. We thank Françoise Besset for her help in preparing some of the figures and carrying out some of the calculations. AC was supported by a grant from NOAA, and CF by a Grant from the PNEDC and the SINTEX and PREDICATE EU project.

APPENDIX A

On the Conservation of Linear Relationships between Two Fields Using MCA

Some caution has been raised concerning the conservation of linear relationships between two fields when using MCA (Newman and Sardeshmuk 1995). The MCA between variables $\mathbf{X}$ (e.g., Z_{500}) and $\mathbf{Y}$ (e.g., SST) uses a singular value decomposition of the covariance matrix $\mathbf{C} = \mathbf{X}\mathbf{Y}^t = \mathbf{U}\mathbf{D}\mathbf{V}^t$, where $\mathbf{U}$ contains the left singular vectors [$\mathbf{u}_k(x)$ in (1)] and $\mathbf{V}$ the right singular vectors [$\mathbf{v}_k(x)$ in (2)], with $\mathbf{U}^t\mathbf{U} = \mathbf{I}$ and $\mathbf{V}^t\mathbf{V} = \mathbf{I}$. Here $\mathbf{D}$ is a diagonal matrix containing the singular values σ_k of $\mathbf{C}$ ($\mathbf{I}$ is the diagonal identity matrix), and t denotes transpose. Newman and Sardeshmuk showed that if $\mathbf{X}$ and $\mathbf{Y}$ are linearly related ($\mathbf{X} = \mathbf{L}\mathbf{Y}$) then the linear relation does not necessarily apply to the left ($\mathbf{U}$) and right ($\mathbf{V}$) singular vectors, that is, we have, in general, $\mathbf{U} \neq \mathbf{L}\mathbf{V}$. Note however that the linear relation still holds between $\mathbf{U}$ and $\mathbf{Y}\mathbf{Y}^t\mathbf{V}$. Multiplying $\mathbf{C} = \mathbf{X}\mathbf{Y}^t$ by $\mathbf{V}$ on the right-hand side yields $\mathbf{C}\mathbf{V} = \mathbf{L}\mathbf{Y}\mathbf{Y}^t\mathbf{V}$, and one also has from above $\mathbf{C}\mathbf{V} = \mathbf{U}\mathbf{D}$. This demonstrates that $\mathbf{U}\mathbf{D} = \mathbf{L}\mathbf{Y}\mathbf{Y}^t\mathbf{V}$, that is, there exists a linear relationship between $\mathbf{U}\mathbf{D}$ (or $\mathbf{U}$) and $\mathbf{Y}\mathbf{Y}^t\mathbf{V}$.

As shown in Bretherton et al. (1992), the relations $\mathbf{Y}\mathbf{Y}^t\boldsymbol{\upsilon}_k = \mathbf{Y}\mathbf{b}_k^t$ and $\sigma_k\mathbf{u}_k = \mathbf{X}\mathbf{b}_k^t$ define the $\mathbf{Y}$-homogeneous and $\mathbf{X}$-heterogeneous covariance maps, respectively, where $\boldsymbol{b}_k$ is the expansion coefficient of $\mathbf{Y}$, as in Eq. (2). As we showed that a linear relation between $\mathbf{X}$ and $\mathbf{Y}$ applies to $\mathbf{Y}\mathbf{Y}^t\boldsymbol{\upsilon}_k$ and $\sigma_k\mathbf{u}_k$, we display the MCA results as homogeneous covariance maps for SST (X) versus heterogeneous covariance maps for Z_{500} (Y). The covariance maps are further scaled by the standard deviation of the expansion coefficient $\boldsymbol{b}_k(t)$, so they give the typical amplitudes of SST and height changes at 500 mb associated with the MCA.

APPENDIX B

Origin of the NAH Pattern

The seasonality of the NAH pattern (the lag −4 SST pattern in Fig. 5) can be estimated by projection onto sets of three successive months. Figure B1 (continuous line) shows that its amplitude depends weakly on season, although there is a maximum in late spring–early summer and a minimum in winter.[1] It is thus not surprising that the NAH pattern turns out to be very similar (and explaining a similar amount of variance) to the

[1] The amplitude shown in Fig. B1 represents a spatially averaged anomaly over the domain. Local values may be larger.

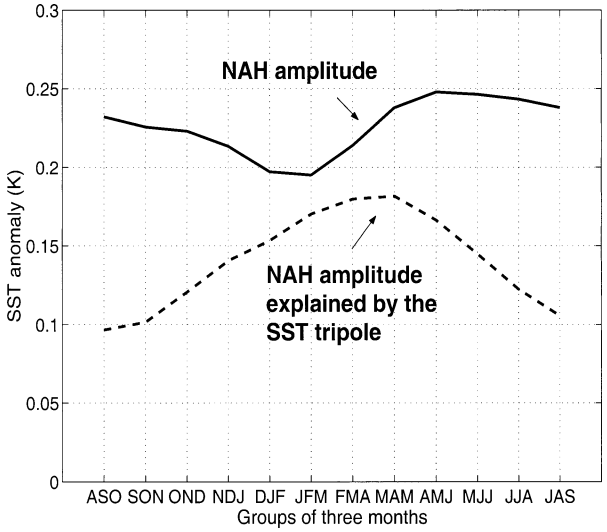

FIG. B1: Amplitude (in K, continuous curve) of the NAH pattern along the course of a year. The dashed curve shows the amplitude of the NAH pattern resulting from its spatial correlation with the SST tripole. For each group of three months, the amplitude A is computed from $A = (\alpha \times \sigma_{\text{tot}}^2)^{1/2}$ where α is the fraction of explained variance by NAH or the tripole, and σ_{tot}^2 is the basin-averaged total variance.

second EOF of the monthly SST anomalies from May–October.

As the NAH and tripole SST anomaly patterns are spatially correlated (0.57), the tripole projects strongly onto the NAH pattern, and a fraction of the NAH amplitude in winter results from the large amplitude of the tripole in this season. To estimate this fraction, we have superimposed in Fig. B1 the seasonal amplitude of the tripole, after multiplication by 0.57 (dashed line). It shows that from DJF to MAM more than 75% of the NAH amplitude can be explained by the tripole, with a 87% peak in JFM. During the warm season, Fig. B1 indicates that typically 40% of the NAH amplitude can be explained by its projection onto the tripole.

The NAH pattern thus only appears to be a genuine SST anomaly mode in summer and fall. To investigate the mechanisms that are responsible for its generation, we computed the correlation between the NAH time series and surface winds and 500-mb height field during these seasons. The correlations are stronger when the atmosphere precedes by 1 month than when it is in phase, suggesting that the correlation maps at a 1-month lag reflects the atmospheric forcing of NAH (Fig. B2). In both seasons, a cyclonic circulation anomaly at the surface and in the midtroposhere roughly centered at 40°N–40°W overlies the cold SST anomaly found 1 month later southeast of Newfoundland. The increased cyclonicity over the basin is certainly instrumental in governing the cold SST anomaly near 40°N–40°W since (i) it favors the entrainment of colder waters through Ekman processes acting on the shallow summer–fall mixed layer; (ii) it is likely to be associated with increased cloudiness over the ocean. At the same time, a reduction of the strength of the trade winds, which reduces the evaporation, precedes the warm SST anomaly along the eastern subtropics. The origin of the warming along the northeastern Atlantic is less clear, as the local surface wind anomalies differ between fall (Fig. B2a) and summer (Fig. B2b). In any case, as the summer pattern at 500 mb (Fig. B2b) explains a significant fraction (25%) of the Z_{500} variance during this season, the

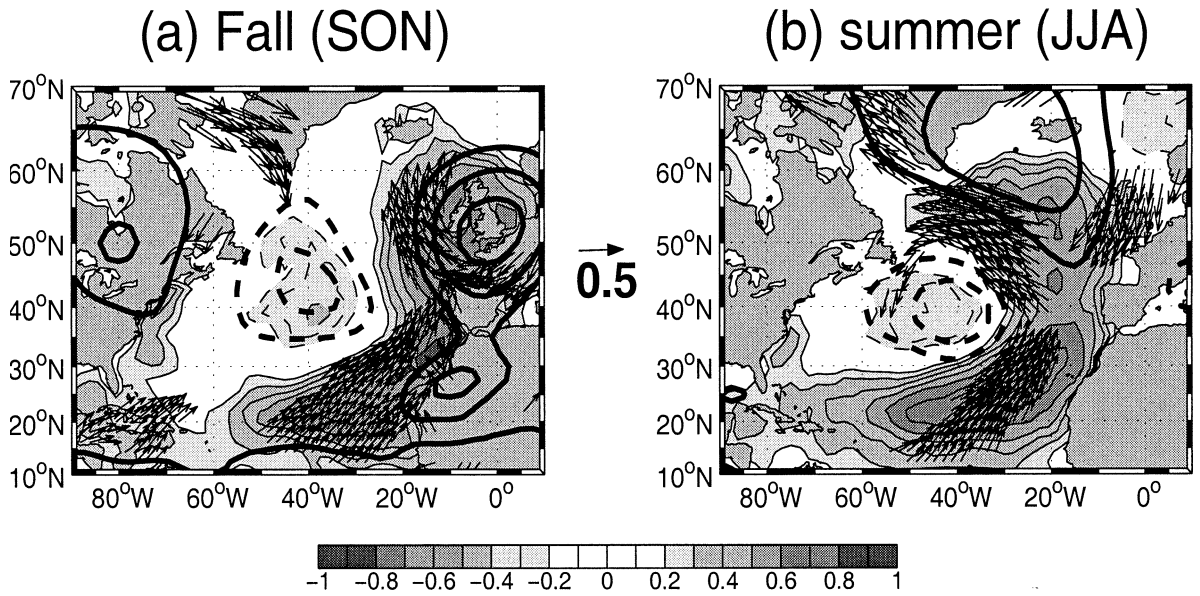

FIG. B2: Correlation map of Z_{500} (contoured every 0.1, starting at ± 0.2, dashed for negative), surface wind stress (arrow, with only vectors of norm >0.3 plotted), SST (gray shading, dashed for negative contours) with the MCA–SST time series found in the analysis of Fig. 5 at (a) lag -2 (SST in SON) and (b) lag -5 (SST in JJA). The atmospheric fields are taken one month before the SST.

NAH pattern during the warm season results from the summertime atmospheric variability.

REFERENCES

Bretherton, C. S., and D. S. Battisti, 2000: An interpretation of the results from atmospheric general circulation models forced by the time history of the observed sea surface temperature distribution. *Geophys. Res. Lett.,* **27,** 767–770.

——, C. S. Smith, and J. M. Wallace, 1992: An intercomparison of methods for finding coupled patterns in climate data. *J. Climate,* **5,** 541–560.

Cayan, D., 1992: Latent and sensible heat flux anomalies over the northern oceans: Driving the sea surface temperature. *J. Phys. Oceanogr.,* **22,** 859–881.

Czaja, A., and C. Frankignoul, 1999: Influence of the North Atlantic SST anomalies on the atmospheric circulation. *Geophys. Res. Lett.,* **26,** 2969–2972.

——, and J. Marshall, 2000: On the interpretation of AGCMs response to prescribed time-varying SST anomalies. *Geophys. Res. Lett.,* **27,** 1927–1930.

——, and ——, 2001: Observations of atmosphere–ocean coupling in the North Atlantic. *Quart. J. Roy. Meteor. Soc.,* **127,** 1–24.

Deser, C., and M. L. Blackmon, 1993: Surface climate variations over the North Atlantic Ocean during winter: 1900–1989. *J. Climate,* **6,** 393–408.

——, and M. S. Timlin, 1997: Atmosphere–ocean interaction on weekly timescales in the North Atlantic and Pacific. *J. Climate,* **10,** 393–408.

Frankignoul, C., 1985: Sea surface temperature anomalies, planetary waves and air–sea feedbacks in the middle latitude. *Rev. Geophys.,* **23,** 357–390.

——, and K. Hasselmann, 1977: Stochastic climate models. Part II: Application to sea-surface temperature variability and thermocline variability. *Tellus,* **29,** 289–305.

——, A. Czaja, and B. L'Hévéder, 1998: Air–sea feedback in the North Atlantic and surface boundary conditions for ocean models. *J. Climate,* **11,** 2310–2324.

Hoerling, M. P., J. W. Hurrell, and T. Xu, 2001: Tropical origins for recent North Atlantic climate change. *Science,* **292,** 90–92.

Horel, J. D., and J. M. Wallace, 1981: Planetary-scale atmospheric phenomena associated with the Southern Oscillation. *Mon. Wea. Rev.,* **109,** 813–829.

Hurrell, J. W., 1995: Decadal trends in the North Atlantic Oscillation: Regional temperatures and precipitation. *Science,* **269,** 676–679.

Kalnay, E., and Coauthors, 1996: The NCEP/NCAR 40-Year Reanalysis Project. *Bull. Amer. Meteor. Soc.,* **77,** 437–471.

Latif, M., K. Arpe, and E. Roeckner, 2000: Oceanic control of decadal North Atlantic sea level pressure variability in winter. *Geophys. Res. Lett.,* **27,** 727–730.

Mehta, V., M. Suarez, J. V. Manganello, and T. D. Delworth, 2000: Oceanic influence on the North Atlantic Oscillation and associated Northern Hemisphere climate variations: 1959–1993. *Geophys. Res. Lett.,* **27,** 121–124.

Namias, J., 1964: Seasonal persistence and recurrence of European blocking during 1958–60. *Tellus,* **3,** 394–407.

Newman, M., and P. D. Sardeshmukh, 1995: A caveat concerning singular value decomposition. *J. Climate,* **8,** 352–360.

Ratcliffe, R. A., and R. Murray, 1970: New lag associations between North Atlantic sea temperature and European pressure applied to long-range weather forecasting. *Quart. J. Roy. Meteor. Soc.,* **96,** 226–246.

Robertson, A. W., C. R. Mechoso, and Y. J. Kim, 2000: The influence of Atlantic sea surface temperature anomalies on the North Atlantic oscillation. *J. Climate,* **13,** 122–138.

Robinson, W. A., 2000: Review of WETS—The Workshop on Extratropical SST anomalies. *Bull. Amer. Meteor. Soc.,* **81,** 567–577.

Rodwell, M. J., and C. K. Folland, 2001: Atlantic air–sea interaction and seasonal predictability, *Quart. J. Roy. Meteor. Soc.,* in press.

——, D. P. Rowell, and C. K. Folland, 1999: Oceanic forcing of the wintertime North Atlantic Oscillation and European climate. *Nature,* **398,** 320–323.

von Storch, H., and F. W. Zwiers, 1999: *Statistical Analysis in Climate Research.* Cambridge University Press, 499 pp.

Wallace, J. M., and D. S. Gutzler, 1981: Teleconnections in the geopotential height field during the Northern Hemisphere winter. *Mon. Wea. Rev.,* **109,** 784–812.

——, C. Smith, and Q. Jiang, 1990: Spatial patterns of atmosphere–ocean interaction in the Northern Hemisphere. *J. Climate,* **3,** 990–998.

Watanabe, M., and M. Kimoto, 2000: Ocean atmosphere thermal coupling in the North Atlantic: A positive feedback. *Quart. J. Roy. Meteor. Soc.,* **126,** 3343–3369.

Zebiak, S. E., 1993: Air–sea interaction in the equatorial Atlantic region. *J. Climate,* **6,** 1567–1586.